Dominant-negative *TP53* mutations potentiated by the HSF1-regulated proteostasis network

Rebecca M. Sebastian[1], Jessica E. Patrick[1], Tiffani Hui[2], David R. Amici[3,4,5,6], Andrew O. Giacomelli[7], Vincent L. Butty[8], William C. Hahn[9,10], Marc L. Mendillo[3,4,5], Yu-Shan Lin[2], Matthew D. Shoulders[1,10,11,12]

[1]Department of Chemistry, Massachusetts Institute of Technology, Cambridge, MA, USA
[2]Department of Chemistry, Tufts University, Medford, MA, USA
[3]Department of Biochemistry and Molecular Genetics, Northwestern University Feinberg School of Medicine, Chicago, IL, USA
[4]Simpson Querrey Institute for Epigenetics, Northwestern University Feinberg School of Medicine, Chicago, IL
[5]Robert H. Lurie Comprehensive Cancer Center, Northwestern University Feinberg School of Medicine, Chicago, IL
[6]Medical Scientist Training Program, Northwestern University Feinberg School of Medicine, Chicago, IL
[7]Humber Polytechnic, Toronto, ON, Canada
[8]BioMicro Center, Massachusetts Institute of Technology, Cambridge, MA, USA
[9]Dana-Farber Cancer Institute, Boston, MA, USA
[10]Broad Institute of MIT and Harvard, Cambridge, MA, USA
[11]Koch Institute for Integrative Cancer Research, Massachusetts Institute of Technology, Cambridge, MA, USA
[12]To whom correspondence may be addressed:
Matthew D. Shoulders
Department of Chemistry
Massachusetts Institute of Technology
77 Massachusetts Avenue, 16-573A
Cambridge, MA 02139
Phone: (617)452-3525
Email: mshoulde@mit.edu

ABSTRACT

Protein mutational landscapes are sculpted by the impacts of the resulting amino acid substitutions on the protein's stability and folding or aggregation kinetics. These properties can, in turn, be modulated by the composition and activities of the cellular proteostasis network. Heat shock factor 1 (HSF1) is the master regulator of the cytosolic and nuclear proteostasis networks, dynamically tuning the expression of cytosolic and nuclear chaperones and quality control factors to meet demand. Chronic increases in HSF1 levels and activity are prominent hallmarks of cancer cells. One plausible explanation for this observation is that the consequent upregulation of proteostasis factors could biophysically facilitate the acquisition of oncogenic mutations. Here, we experimentally evaluate the impacts of chronic HSF1 activation on the mutational landscape accessible to the quintessential oncoprotein p53. Specifically, we apply quantitative deep mutational scanning of p53 to assess how HSF1 activation shapes the mutational pathways by which p53 can escape cytotoxic pressure conferred by the small molecule nutlin-3, which is a potent antagonist of the p53 negative regulator MDM2. We find that activation of HSF1 broadly increases the fitness of dominant-negative substitutions within p53. This effect of HSF1 activation was particularly notable for non-conservative, biophysically unfavorable amino acid substitutions within buried regions of the p53 DNA-binding domain. These results indicate that chronic HSF1 activation profoundly shapes the oncogenic mutational landscape, preferentially supporting the acquisition of cancer-associated substitutions that are biophysically destabilizing. Along with providing the first experimental and quantitative insights into how HSF1 influences oncoprotein mutational spectra, these findings also implicate HSF1 inhibition as a strategy to reduce the accessibility of mutations that drive chemotherapeutic resistance and metastasis.

INTRODUCTION

Cancers typically arise by multi-step acquisition of genetic alterations that dysregulate cell growth and survival programs, leading to malignant phenotypes that promote and sustain prototypical hallmarks of cancer[1-3]. In addition to mutated genes, cancer cells also co-opt non-mutated genes within stress pathways to aid cell growth, in a process known as non-oncogene addiction[4, 5]. Particularly noteworthy in this regard, pathways associated with regulation of proteostasis are upregulated in cancer, likely owing to challenges arising from dysregulated protein synthesis, nutrient starvation, subunit imbalance within protein complexes resulting from aneuploidy, and, perhaps, expression of oncoproteins with destabilizing amino acid substitutions[6-12].

Among the most frequently upregulated proteostasis stress pathways in cancer is the heat shock response (HSR), which is controlled by the master transcription factor HSF1[13, 14] — a transcription factor that can also modulate additional cell remodeling programs in tumors[15-17]. Constitutive overexpression of heat shock proteins regulated by HSF1 is widely observed in malignant cells[6, 14, 18], as are overexpression and constitutive activity of HSF1 itself[14-16, 19, 20]. Notably, HSF1 supports the emergence of tumors in mice following exposure to mutagens, and high levels of HSF1 expression are associated with increased mortality rates in breast cancer[19, 21, 22]. Additionally, HSF1 and the HSF1-regulated chaperone heat shock protein 90 (HSP90) facilitate the emergence of resistance to chemotherapeutic agents, although molecular-level mechanisms of this effect are currently unclear[23-25]. In sum, much attention has been drawn not just to HSP90[26-29] but also to HSF1 as a potential chemotherapeutic target, motivating the development of potent small molecules that target HSR components either specifically through inhibition of individual chaperones or broadly through targeting HSF1 itself[30-33].

Successful emergence of gain-of-function mutations in all proteins[34], including gain-of-function in oncoproteins that play critical roles in tumor progression and disease maintenance, is constrained by the biophysical properties of the evolving protein, particularly as most functionally important amino acid substitutions are non-conservative and therefore often biophysically deleterious[35]. One intriguing hypothesis is that the proteostasis environment itself defines the accessibility of novel mutations by regulating the folding and degradation of the resulting protein variants. A growing body of literature has focused on the impact of proteostasis network components, and in particular chaperones such as HSP90 and HSP70, on protein evolution as organisms and viruses adapt[34, 36-44]. Among other advances, such studies have shown that proteostasis network remodeling mediated by stress-responsive transcription factors can have major impacts on the mutational space accessible to viral pathogens that parasitize host chaperones[40-43], and that these effects are often mediated directly by the influence of proteostasis network composition on client protein folding and stability[34, 38, 42, 45].

Building on these studies, one compelling possibility regarding the roles of HSF1 in cancer is that HSF1 overexpression may support malignancy by creating a permissive protein folding environment that directly facilitates the emergence of proliferation-promoting oncogenic mutations. Such a role for HSF1 in defining accessible oncogenic mutations has never been experimentally explored.

The tumor suppressor p53 is a key transcription factor and regulator of the response to DNA-damage and other oncogenic stimuli. When activated, p53 induces cell-cycle arrest, senescence or apoptosis[46]. p53 is the most frequently mutated gene in cancer[47]. Indeed, mutations in p53 occur in >50% of tumors[48, 49]. The majority of these mutations are missense mutations within p53's DNA-binding domain[48]. While some p53 missense mutations confer a loss-of-function effect typical of tumor suppressors, mutations in p53 can also function via a dominant-negative effect in which the mutated p53 allele encodes a protein variant that inhibits the function of residual wild-type p53 through either heterotetramerization via a C-terminal oligomerization domain or by inducing co-aggregation and consequent loss-of-function[50-52]. Dominant-negative p53 variants can be further classified as either DNA-contact mutations that impact DNA association but cause minimal structural perturbations, or conformational mutations that initiate global or local unfolding of the DNA-binding domain[53-56].

p53 interacts extensively with the HSF1-regulated chaperones HSP90 and HSP70, which in turn regulate the stability and activity of p53[57-60]. Notably, while wild-type p53 interacts transiently with cytosolic chaperones, particularly during folding and maturation, several mutant alleles of p53 display more stable interactions with HSP70 and HSP90, contributing to increased mutant p53 levels[61-65]. Considering p53's premier role in diverse cancers, the large number of destabilizing p53 mutations that lead to pro-oncogenic dominant-negative behavior, and the extensive interactions between p53 and HSF1-regulated chaperones, p53 represents a compelling model system to explore impacts of HSF1 activation on oncogenic evolution.

In this study, we applied deep mutational scanning (DMS) of p53 in concert with chemical genetic regulation of HSF1 to examine the impacts of proteostasis modulation on the fitness of dominant-negative p53 variants that can drive cancer. We observed that constitutive activation of HSF1 broadly increases the fitness of diverse dominant-negative p53 mutations, including several mutations within hot-spot sites frequently associated with cancer. The impact of HSF1 activation on p53's mutational spectrum was most evident in the context of non-conservative substitutions of hydrophobic amino acids from non-polar to polar and charged amino acids within buried regions of p53's DNA-binding domain. These substitutions are also most likely to be biophysically destabilizing and folding-disruptive, consistent with the notion that activation of HSF1 increases the fitness of mutations that perturb p53 stability or folding. Altogether, these results indicate that HSF1 can directly potentiate oncogenic evolution by

opening access to otherwise biophysically problematic amino acid sequences. Further, they suggest that both HSF1 inhibition specifically and proteostasis network inhibition more broadly as a potent therapeutic strategy to prevent acquisition of resistance mutations during chemotherapy.

RESULTS

TP53 mutational library integrated with chemical genetic regulation of the HSR

To assess the impacts of HSF1 on the mutational landscape of dominant-negative p53, we first needed to establish a system in which HSF1 activity could be robustly regulated in an appropriate cell line. We chose to use A549 cells as an epithelial tumor model, as they are derived from a human alveolar basal cell adenocarcinoma[66]. Importantly, A549 cells exclusively express wild-type p53, critically enabling our experimental workflow[67]. Pharmacologic activation of HSF1 is traditionally achieved via treatment with Hsp90 or Hsp70 inhibitors or toxins like arsenite[68]. Such approaches are not useful here, as they activate HSF1 indirectly by causing massive cellular protein misfolding, and ultimately drive apoptosis via proteostatic overload. To overcome this issue, we employed regulated expression of a constitutively active HSF1 variant, termed cHSF1. Specifically, we constructed a stable, single-colony A549 cell line in which cHSF1 expression was placed under the control of a doxycycline (dox)-responsive promoter[69-72]. In these cells, which we termed A549^{cHSF1} cells, treatment with dox activates expression of cHSF1, which then proceeds to upregulate HSR-controlled gene expression independent of protein misfolding stress.

To test the activation of HSF1, we treated A549^{cHSF1} cells with dox or vehicle for 24 h and then evaluated the transcript levels of established HSF1 target genes using qPCR. In our optimized cell line, we observed modest upregulation of HSP40 and HSP70 transcripts during HSF1 activation as compared to vehicle treatment, indicating that our cHSF1 construct was functionally modulating the HSR as intended (**Figures 1A** and **1B**). Critically, we selected cells in which HSF1 induction upregulated HSR genes to levels that are still well within the physiologically accessible regime, a feature that is known to be critical to avoid off-target induction of genes not normally targeted by HSF1[71, 73]. For example, treatment with STA-9090[74], an HSP90 inhibitor and robust activator of endogenous HSF1 had considerably stronger effects than did dox treatment (**Figures 1A** and **1B**). Moreover, a resazurin metabolic activity assay[75] indicated that cell growth and viability were not substantially altered by dox-mediated HSF1 induction (**Figure S1A**).

We transduced these A549^{cHSF1} cells with a high-quality, lentiviral-based p53 mutational library in which all possible single amino acid substitutions across the p53 gene are present[50, 76]. We performed the transduction at a very low multiplicity of infection to ensure that a single mutant p53 variant was expressed in each cell, alongside endogenous wild-type p53 (**Figure 1C**). To evaluate the diversity of the resulting A549^{cHSF1} p53 variant library, which we termed A549^{cHSF1}(p53-Lib) cells, we harvested genomic DNA from the A549^{cHSF1}(p53-Lib) cells, and then amplified the library-encoded *TP*53 gene us-

ing PCR before deep-sequencing. Out of 7467 potential missense mutations generated from 19 possible amino acid substitutions at 393 sites, 7465 (99.9%) of the possible substitutions were observed with a read depth >10 counts per amino acid substitution (**Figure S1B** and **Table S1**).

HSF1 activation modulates the p53 mutational landscape during nutlin-3 selection

We next sought to apply DMS to test whether HSF1 activity alters tolerance for p53 mutations that promote escape from nutlin-3 selection. Our approach was to perform selections in the HSF1-enhanced or the basal proteostasis environment in the presence of the p53-activating agent nutlin-3[76]. Nutlin-3 inhibits the interaction between p53 and mouse double minute 2 homolog (MDM2), an E3 ubiquitin ligase and a negative regulator of p53[77]. In unstressed cells, MDM2 binds to p53 to induce ubiquitination and degradation. Binding of nutlin-3 to MDM2 releases p53 from the MDM2 complex, allowing p53 to accumulate and induce a transcriptional program that drives apoptosis and cell cycle arrest. Cells that express an introduced dominant-negative p53 variant alongside endogenous wild-type p53 are strongly positively selected in the presence of nutlin-3, because dominant-negative p53 attenuates the wild-type p53-mediated activation of cell cycle arrest and thereby allows cells to continue to proliferate, even in the presence of nutlin-3 (**Figure 2A**).

We treated A549^{cHSF1}(p53-Lib) cells with nutlin-3 (or vehicle) in the context of either a basal or a HSF1-activated proteostasis environment, allowing the selection to proceed under these conditions over a 12-day period[76]. After selection, we followed a published protocol to deep-sequence the library-encoded *TP53* amplicons[76]. We next calculated the resulting changes in p53 variant frequency as the $\log_2$ fold-change in normalized read counts of amino acid substitutions between our various selection versus control conditions. The resulting mutational and site-level $\log_2$ fold-change values are available in **Tables S2** and **S3**.

We expected that nutlin-3 would be the dominant force affecting the fitness of p53 variants, as cells that fail to express a dominant-negative p53 variant cannot survive nutlin-3 selection. Consistent with this expectation, we observed a very strong and positive enrichment of missense mutations within the DNA-binding domain of p53, located from residues 100–300, upon nutlin-3 selection in both the basal (**Figure S2A**) and the HSF1-activated (**Figure S2B**) proteostasis environments relative to the corresponding vehicle-treated (no nutlin-3) controls. Importantly, the sites enriched during this nutlin-3 selection in both the basal and HSF1-activated environments overlapped with previous selections for dominant-negative p53 using saturation mutagenesis in both the A549 and AML cell lines[50, 76]. Moreover, the fitness of p53 variants identified as somatic mutations within the IARC (International Agency for Research on Cancer, R20)[78] database was higher as compared to *TP53* mutations absent from the data-

base, confirming that nutlin-3 was selecting for the expected, cancer-associated *TP53* mutations (**Figures S2C** and **S2D**). We also observed an exceptionally high degree of correlation for the cumulative site $\log_2$ fold-change values between biological replicates of nutlin-3 treatment (**Figure S3**), further indicating the very large magnitude of the selection pressure endowed by nutlin-3 treatment.

Next, to isolate the impact of HSF1 activation on dominant-negative p53 mutational tolerance, we evaluated whether and how HSF1 activation affected p53 variant fitness specifically during nutlin-3 selection. We observed a striking increase in p53 variant fitness across much of the *TP53* gene during HSF1 activation (**Figure 2B**). The correlation between individual replicates, shown in **Figure S4A**, was positive and highly significant, indicating the results were reproducible. That said, while reasonable for a DMS experiment[41-43, 79-81], the correlation was not as strong as the correlation observed for nutlin-3 treatment versus control, an observation that is consistent with the absolute nature of nutlin-3 selection that leads to a very large effect size for that treatment.

The observation that chronic HSF1 activation, which is commonly observed across diverse cancers[13-17, 19, 20], broadly increased p53 mutational tolerance (**Figure 2B**) motivated us to analyze the underlying effect in greater depth. We first subdivided variants by domain and examined the distribution of the net site $\log_2$ fold-change for mutations that encoded amino acid substitutions within each domain. In all functional domains examined, we observed a significant and often substantial increase in net site fitness (**Figure 2C**). One potential explanation for such a global increase in variant fitness could be non-specific increases in cell viability and proliferation during nutlin-3 treatment as a result of HSF1 activation—increases not associated with direct effects on p53 variant fitness. If such were the case, we would expect to see an increase for silent mutations as well as missense mutations. To address this possibility, we compared the fitness of missense mutations to silent mutations within each p53 domain (**Figure 2D**). Across all domains, we observed an HSF1-dependent increase in mutational fitness for missense mutations only. HSF1 had no meaningful impact on silent mutations. Also noteworthy, HSF1 had minimal effects on p53 variant enrichment in the absence of nutlin-3 treatment to provide a driving force for p53 selection (**Figure S4B**). These observations strongly support the interpretation that HSF1 activation is specifically enhancing the fitness of non-synonymous *TP53* mutations, and that this phenomenon is driven by direct effects of HSF1 activation on the resulting p53 variants rather than general effects on cell fitness.

We next examined the impacts of HSF1 activation during nutlin-3 treatment on variant fitness within the p53 DNA-binding domain (**Figures 3A**, **3B**, and **S5**), as the majority of known oncogenic *TP53* mutations are localized to this region[78]. Moreover, the DNA-binding domain is the most robustly characterized region of p53, with ample high-resolution structural information available to enable more

detailed analyses. The p53 DNA-binding domain is composed of a core β-sandwich scaffold supporting a DNA-binding surface comprising two loops (Loop 2 and Loop 3) stabilized by Zn^{2+} coordination, as well as a loop-sheet-helix motif that contains Loop 1[82]. The most dramatic consequences of HSF1 activation in this region occurred in sites 238–249 within Loop 3, as well as at sites V173 and H179 within Loop 2 (**Figure S5**). Interestingly, several cancer hot spots are localized in this region, including sites G245, R248, and R249, all of which displayed a net increase in fitness upon HSF1 activation (**Figure 3B)**. These observations indicate that HSF1 can directly support the acquisition of hot-spot mutations in p53 that lead to malignant transformation.

Zn^{2+} coordination is critical for p53's ability to bind DNA, and loss of Zn^{2+} binding is associated with destabilization and aggregation of p53[53, 83, 84]. We therefore next examined the fitness of amino acid substitutions within the Zn^{2+} coordination sites (C176 and H179 of Loop 2 and C238 and C242 of Loop 3; **Figure 3B**). As with other cancer-associated mutations, we observed that the net site fitness for all four coordinating residues was increased following HSF1 activation.

Relatively fewer p53 sites displayed an overall net negative fitness upon HSF1 activation during nutlin-3 treatment. Interestingly, several of the few sites with net negative fitness (V172, R174, and T211; **Figure 3B**) are localized at the surface of a pocket, which interacts with the N-terminal tail of the DNA-binding domain. Interaction of the N-terminal tail of the DNA-binding domain with residues in this pocket has been shown to both increase p53 thermodynamic stability as well as decrease aggregation propensity[85-87]. A possible explanation for the decrease in fitness at these specific sites is that variants within this region increase the propensity for mutant p53 to co-aggregate with wild-type p53, with resultant dominant-negative consequences favorable in nutlin-3 selection. Such destabilization and aggregation may be attenuated in the supportive proteostasis environment created by HSF1 activation, leading to their relative decrease in fitness in combinatorial selection.

HSF1 activation supports the accumulation of biophysically non-conservative amino acid substitutions within buried sites

Prototypical oncogenic p53 amino acid substitutions can be classed into either DNA-contact variants with minimal impact on thermodynamic stability or structural mutations that significantly perturb the stability of the DNA-binding domain[53]. Mutations within this second class are frequently localized to either the Zn^{2+}-binding site, discussed above, or within the β-sandwich motif at the hydrophobic core of the DNA-binding domain. Thus, we next asked whether there was a correlation between relative solvent accessibility (RSA; **Table S4**) and net site fitness within the p53 DNA binding domain during nutlin-3-mediated p53 selection. Indeed, when we examined the RSA of sites during nutlin-3 selection versus vehicle treatment in either the basal or in the HSF1-activated proteostasis environment, we observed a

negative correlation between net site fitness and RSA (**Figures S6A–D**). This observation is consistent with the hypothesis that amino acid substitutions in buried regions of the p53 DNA-binding domain are more likely to induce a dominant-negative effect than substitutions within surface-exposed residues.

We next asked whether enhancing the proteostasis network via HSF1 activation during nutlin-3 selection preferentially impacted the fitness of p53 amino acid substitutions within buried regions of the p53 DNA-binding domain. Variants classified as buried (RSA < 0.2) did display marginally higher net fitness as compared to sites that were exposed (RSA > 0.2) (**Figure 4A**). Motivated by this intriguing result, we clustered variants into (a) conservative amino acid substitutions, (b) non-conservative substitutions from a nonpolar to a charged amino acid, and (c) non-conservative substitutions from a charged to a nonpolar amino acid and separated them based on whether they occurred in buried versus exposed p53 sites. Then, we analyzed whether HSF1 activation impacted non-conservative substitutions more strongly than conservative substitutions. There was no significant effect of HSF1 activation on conservative or either class of non-conservative p53 substitutions in exposed regions. Strikingly, however, non-conservative substitutions replacing a non-polar amino acid with a charged or polar amino acid within buried p53 sites displayed substantially and significantly higher fitness upon HSF1 activation relative to either conservative substitutions or non-conservative substitutions from polar to non-polar amino acids in buried regions (**Figure 4B**). These results strongly support the notion that HSF1 activation is allowing p53 to more robustly access otherwise biophysically disfavored regions of its mutational landscape.

HSF1 activation specifically enhances the fitness of destabilizing mutations in buried regions of the p53 DNA-binding domain

Since we observed a preferential impact on variant fitness for non-conservative substitutions within buried p53 residues (**Figure 4B**), and given that non-conservative substitutions within buried regions of a protein would be expected to frequently reduce protein stability, we next sought to assess whether HSF1 selectively enhanced the fitness of p53 variants with reduced thermodynamic stability. We first examined the impact of HSF1-activated versus basal proteostasis environments during nutlin-3 selection on 42 missense mutations in the p53 DNA-binding domain for which thermodynamic stability has been experimentally determined[53, 88-90]. We grouped the variants into those that were neutral or stabilizing ($\Delta\Delta G$ < 0.5 kcal/mol) or those that were destabilizing ($\Delta\Delta G$ > 0.5 kcal/mol). We observed a suggestive, but not statistically significant, increase in fitness for mutations that were thermodynamically destabilizing as compared to neutral or stabilizing mutations (**Figure 5A**).

As only a very limited number of p53 DNA-binding domain variants have experimentally determined thermodynamic stability measurements, we next sought to use Rosetta to estimate the change in

thermodynamic stability for all possible amino acid substitutions within the DNA-binding domain[91]. To assess the accuracy of the calculated $\Delta\Delta G$ values, we first compared the computed to the experimentally determined $\Delta\Delta G$ values for the aforementioned 42 amino acid substitutions. We observed strong correlation between the two approaches (**Figure S7A**). With the computational approach validated, we next examined whether p53 variants enriched during nutlin-3 selection were associated with a decrease in estimated stability (**Table S5**). We observed that amino acid substitutions with a greater estimated $\Delta\Delta G$ were associated with higher fitness during nutlin-3 selection in both the basal and HSF1-activated proteostasis environments, independently of whether mutations were located within buried or exposed sites (**Figures S7B** and **C**).

We next assessed whether HSF1 activation preferentially impacted thermodynamically destabilizing amino acid substitutions in the p53 DNA-binding domain. First, we binned variants into those where HSF1 activation either increased or decreased fitness during nutlin-3 selection to evaluate whether there was a difference in estimated thermodynamic stability between the two groups. Strikingly, in buried p53 regions we observed that substitutions whose fitness was enhanced by HSF1 activation were more likely to display a higher estimated $\Delta\Delta G$ than variants that displayed decreased fitness (**Figure 5B**). In contrast, no significant difference in the effect of HSF1 activation on destabilized versus stabilized variants was observed for exposed sites in p53 (**Figure 5B**). Consistent with this observation, there was an overall positive and significant correlation between variant fitness during HSF1 activation and estimated $\Delta\Delta G$ for buried sites, whereas exposed p53 sites displayed a slight negative correlation (**Figures 5C** and **D**).

Since we had previously observed that HSF1 particularly enhanced the fitness of non-conservative nonpolar-to-polar and charged substitutions in those same regions (**Figure 4B**), we next asked whether we observed a similar effect using this thermodynamic stability approach. Indeed, we observed that substitutions from non-polar to polar charged amino acids in buried regions had by far the greatest impact on estimated stability in buried regions (**Figure 5E**), correlating with the trend we observed when examining the variant fitness effects of HSF1 activation (**Figure 4B**). Taken together, these observations indicate that non-conservative substitutions in buried regions of the p53 DNA-binding domain are destabilizing and are therefore likely impacted by HSF1 activation during nutlin-3 selection owing to their impacts on protein structure and stability. In particular, HSF1 activation directly and preferentially increases the fitness of these same non-conservative and destabilizing substitutions.

HSF1 transcriptional targets overlap with the p53 interactome

We next asked why HSF1 activation preferentially increased the fitness of thermodynamically destabilizing p53 substitutions in the context of nutlin-3 selection. One likely possibility is that HSF1 activation is driving the upregulation of p53 binding partners, particularly those involved in p53 proteostasis. We first assessed exactly how HSF1 activation remodeled the proteostasis network by identifying differentially impacted transcriptional pathways. We treated A549^{cHSF1} cells with dox for 24 h and quantified differentially transcribed genes using RNA-seq. 159 transcripts were significantly differentially expressed with >1.5 fold-change upon HSF1 activation as compared to the vehicle-treated control, highlighting that HSF1 activation was not massively perturbing the global transcriptome (**Table S6**). As expected, known components of the HSR, including HSP90 and HSP70, were highly enriched among the upregulated transcripts (**Figure 6**). Further, gene set enrichment analysis using the MSigDB c5 collection[92] confirmed that genes related to the HSR were highly enriched following activation of HSF1 (**Table S7**). Notably, known p53-induced genes were not substantially impacted by HSF1 activation.

We next asked to what extent HSF1-upregulated transcripts might directly alter p53 proteostasis. To address this issue, we identified the subset of HSF1-induced transcripts that are known to interact with p53. Of the 159 transcripts that were significantly upregulated by HSF1 activation, 22 (13.8%) encode proteins classified by the APID (Agile Protein Interaction DataAnalyzer) database as interacting with p53 (**Figure 6** and **Table S8**)[93]. Included within these p53-interacting proteins, 17 are either chaperones or co-chaperones, including the well-validated and HSF1-regulated p53 chaperones HSP90 and HSP70. These observations are consistent with the notion that the mechanism by which HSF1 increased the fitness of nutlin-3-selected p53 variants is via modulating the folding or aggregation of mutant p53 through direct interaction with HSF1-modulated chaperones that engage p53.

DISCUSSION

Our findings provide the first evidence that HSF1 increases the fitness of p53 dominant-negative variants that can drive cancer, and specifically enhances access to mutations that can escape the chemotherapeutic agent nutlin-3. Moreover, our analyses of the structured DNA-binding domain show that the p53 mutational fitness-enhancing impact of HSF1 activation is strongly biased towards supporting the emergence of thermodynamically destabilizing substitutions located within buried protein regions. In particular, HSF1 upregulation improves the fitness of non-conservative substitutions in which buried non-polar amino acids are replaced by polar or charged amino acids. These findings are consistent with the notion that HSF1 activation enhances the cellular stability of these otherwise unstable p53 variants. Finally, RNA-seq analysis shows that HSF1-activated genes are enriched in p53-interacting chaperones, consistent with the notion that HSF1 directly impacts the fitness of p53 variants through modulation of folding, aggregation, degradation, or stability of mutant p53 via these HSF1-regulated chaperones.

Amino acid substitutions within p53 that induce mild structural defects within the DNA-binding domain are likely to function through tetramerization with wild-type p53, in which case the presence of one or more non-functional p53 subunits reduces the ability of the overall complex to bind to DNA and induce transcription[51, 94, 95]. Therefore, for p53 to retain a dominant-negative function, it is likely that the impact of HSF1 is not to induce a wild-type conformation for mutant p53, but rather to facilitate the cellular stability of a non-native or even potentially aggregation-inducing conformation. Within tumors, mutant p53 is often found to have elevated expression and increased stability in comparison to wild-type p53[53-55, 96, 97]. p53 stabilization has been attributed in part to an increase in half-life following the association of mutant p53 with the cytosolic chaperones HSP90 and HSP70[57, 63-65, 98, 99]. Given that HSF1 activation upregulates numerous p53-interacting chaperones, including HSP90 and HSP70 themselves, our data are consistent with a mechanism in which increased expression of HSF1-regulated chaperones enhances the fitness of dominant-negative p53 variants by prolonging their half-life in the cell. Alternatively, interaction with HSP70 is known to increase the aggregation of, for example, the dominant-negative R175H p53 variant, suggesting that HSF1 activation may also, in some cases, enhance the formation of mutant and wild-type p53 co-aggregates[62, 100].

It is noteworthy that HSF1 itself may be modulated by p53. Previous work suggests that wild-type versus some p53 variants have opposing influences on HSF1 signaling. Residual wild-type p53 in heterozygous mutant p53 tumor systems is capable of partial suppression of HSF1 activity, thereby necessitating loss of p53 heterozygosity in order to fully stabilize mutant p53 expression[101]. From the other direction, some p53 variants may themselves increase HSF1 activity through stimulating MAPK

signaling pathways[102]. Our data are consistent with the notion that HSF1 over-activation may overcome wild-type p53 suppression to restore the dominant-negative function of mutant p53, potentially amplifying the feed-forward circuit of HSF1 activation and continued oncogenic p53 stabilization. In this regard, it would be interesting to perform a mutational scanning experiment using HSF1 variants expressed from the endogenous locus, which is made possible using PRIME editing[103].

The work presented here is, to our knowledge, the first evidence indicating that HSF1 can directly shape the mutational space accessible for malignant transformation. These results have several interesting implications. While the literature has clearly highlighted HSF1 activation as an oncogenic helper[8, 104, 105], it is yet unclear whether the commonly observed increase in HSF1 expression and activity occurs prior to the onset of tumorigenesis, or whether constitutive HSF1 activation is a consequence of proteome instability arising from accumulated mutations and genomic damage. Our results suggest that activation of HSF1 may facilitate early tumorigenic events by increasing the fitness of oncogenic driver mutations. Secondly, resistance to chemo-therapeutic agents is frequently driven by mutations within the targeted proteins. While both HSF1 upregulation as well as downstream chaperones have been identified as facilitators of chemo-resistance, the mechanism has primarily been associated with alterations in metabolic or autophagy pathways[23, 24, 106-109]. Our results indicate that HSF1 activity may also greatly facilitate chemo-resistance by tuning the accessibility of resistance mutations. Given the recent therapeutic interest in inhibitors of both HSF1 itself and HSF1-regulated chaperones such as HSP90 and HSP70[30-32, 70], these results suggest that such inhibitors may be particularly effective in combination therapy to prolong effective outcomes by reducing the emergence of resistant tumor populations. The capacity of HSF1 or other types of proteostasis network upregulation to tune the stability, folding, and/or aggregation of oncoproteins could have tremendous implications for cancer immunotherapy. Variants with enhanced stability may not be able to be degraded, and thus unable to be efficiently presented to the immune system by MHC-1 proteins. Thus, in accordance with our findings and published work in this field, we reason that downregulation of proteostasis networks may enable a more robust immune response to tumor presenting antigens[110]. Further, we emphasize that the impacts of proteostasis network modulation on oncoprotein mutational spectra are likely to extend far beyond just p53. In sum, these findings should catalyze further essential work to more fully understand how HSF1 shapes the mutational spectra of additional oncoproteins and chemotherapy targets, and the potential of HSF1 itself as a chemotherapeutic target.

ACKNOWLEDGEMENTS

This work was supported by the National Institutes of Health (1R35GM136354 to M.D.S.), (1R01AI168166 to Y.-S.L), and by an American Cancer Society–Ellison Foundation Research Scholar Award (to M.D.S.). Additional support was provided by Koch Institute Support (core) under NIH (core) grant P30-CA14051 from the NIH/NCI and by the MIT CEHS core via the NIH/NIEHS (Grant P30-ES002109).

COMPETING INTERESTS

W.C.H. is a consultant for Thermo Fischer Scientific, Solasta Ventures, KSQ Therapeutics, Frontier Medicines, Jubilant Therapeutics, RAPPTA Therapeutics, Serinus Biosciences, Kestral Therapeutics, Function Oncology, Crane Biotherapeutics and Perceptive. A.O.G. is a consultant for Atlas Venture.

AUTHOR CONTRIBUTIONS

R.M.S. and M.D.S. conceived the project. R.M.S., T.H., A.O.G., Y.-S.L., and M.D.S. designed experiments. R.M.S. and T.H. conducted experiments. A.O.G. and W.C.H. provided key reagents. All authors analyzed results and contributed to writing and/or editing the manuscript. Y.-S.L. and M.D.S. obtained funding and supervised the research.

Materials and Methods

Cell culture. A549 cells were a kind gift from the Prof. William Hahn Lab at Harvard Medical School. Cells were grown in DMEM medium (Corning), supplemented with 10% heat-inactivated fetal bovine serum (FBS, Cellgro) and 1% penicillin/streptomycin/glutamine (Cellgro) at 37 °C with 5% CO_2(g).

Plasmids. To create stable A549^{cHSF1} cell lines, cHSF1[70] was cloned into the pINDUCER20 lentiviral vector (AddGene #44012) using Gateway cloning. pINDUCER20 expresses both a gene of interest under a tetracycline responsive TRE2 promoter as well as a tetracycline activator (rtTA3) under a constitutive promoter, enabling inducible regulation of a gene of interest following a single lentiviral transduction. The *TP53* library was expressed in a modified lentiviral pMT_BRD025 vector (AddGene #113569)[76].

Lentivirus production. LentiX cells (Takara Bio), cultured as described above, were co-transfected with the structural plasmids necessary for virus production (psPAX2 and pMDM2.G from AddGene) along with the lentiviral vectors for either pINDUCER20.cHSF1 or the *TP53* mutational library. Cells were transfected using TransIT-Lenti (Mirus) for 24 h, after which the media was removed and replaced with fresh media. Media containing viral particles was collected at 48 h and cell debris was removed by centrifugation at 500 × *g* for 10 min. Viral supernatant was then aliquoted and stored at –80 °C until use. To measure the titer of the *TP53* library lentivirus, A549 cells were infected with serially diluted virus in 96-well plates. The infected cells were then selected in puromycin (Gibco) for 48 h and surviving cells were quantified using resazurin (Sigma).

Resazurin lentiviral titer assay. A549^{cHSF1} cells were seeded in 96-well plates (Corning) at a density of 3×10^5 cells/well in DMEM medium. The following day media was removed and replaced with viral media containing polybrene at a final concentration of 8 µ/mL. After a 96-h incubation, media was removed and replaced with 100 µL of DMEM containing 0.01 mg/mL resazurin sodium salt (Sigma). After 2 h of incubation, resorufin fluorescence (excitation 530 nm; emission 590 nm) was quantified using a Take-3 plate reader (BioTeK). Experiments were conducted in biological triplicate. Viral titer in transducing units per mL (TU/mL) was calculated as: [(number of cells plated) x (fraction of surviving cells)] / (volume of virus). The average of the calculated TU/mL over the linear range of the assay was used for subsequent calculation of appropriate multiplicity of infection.

Stable cell line engineering. For the construction of A549^{cHSF1} cells, A549 cells were transduced with lentivirus co-encoding a G418-resistance gene and rtTA3 alongside cHSF1 in the presence of 2 µg/mL polybrene (Sigma-Aldrich). Heterostable cell lines were then selected using 1 mg/mL G418 (Enzo Life Sciences). Clonal populations were screened based on functional testing of the cHSF1 construct using

real-time polymerase chain reaction (RT-PCR; described below) with or without 1 μg/mL dox (Alfa Aesar).

Resazurin viability assay. A549^{cHSF1} cells were seeded in 96-well plates (Corning) at a density of 3 × 10^5 cells/well in DMEM medium and then treated with 0.1% DMSO, 1 μg/mL dox, 2.5 μM nutlin-3 (Cayman Chemical Company), or 1 μg/mL dox and 2.5 μM nutlin-3. 48 h post-treatment, media was removed and replaced with 100 μL of DMEM containing 0.01 mg/mL resazurin sodium salt (Sigma). After 2 h of incubation, resorufin fluorescence (excitation 530 nm; emission 590 nm) was quantified using a Take-3 plate reader (BioTeK). Experiments were conducted in biological triplicate.

RT-PCR. A549^{cHSF1} cells were treated with 1 μg/mL dox for 24 h for assessment of cHSF1 construct function, while a 6 h treatment with 500 nM STA-9090 (MedChem Express) was used as a positive control for HSR activation. RNA was extracted using the EZNA Total RNA Kit I (Omega). qRT-PCR reactions were performed on cDNA prepared from 1000 ng of total cellular RNA using the High-Capacity cDNA Reverse Transcription Kit (Applied Biosystems). The Fast Start Universal SYBR Green Master Mix (Roche) and appropriate primers purchased Sigma were used for amplifications (6 min at 95 °C then 45 cycles of 10 s at 95 °C, 30 s at 60 °C) in a Light Cycler 480 II Real-Time PCR machine. The primers used for *DNAJB1* were 5′-TGTGTGGCTGCACAGTGAAC-3′ (forward) and 5′-ACGTTTCTCGGGTGTTTTGG-3′ (reverse), primers for *HSPA1A* were 5′-GGAGGCGGAGAAGTACA-3′ (forward) and 5′- GCTGATGATGGGGTTACA-3′ (reverse), primers for *HSP90AA1* were 5′-GATAAACCCTGACCATTCC -3′ (forward) and 5′-AAGACAGGAGCGCAGTTTCATAAA-3′ (reverse) and primers for *RPLP2* were 5′-CCATTCAGCTCACTGATAACCTTG-3′ (forward) and 5′-CGTCGCCTCCTACCTGCT-3′ (reverse). Transcripts were normalized to the housekeeping genes *RPLP2*. All measurements were performed in technical triplicate. Data were analyzed using the LightCycler® 480 Software, Version 1.5 (Roche) and data are reported as the mean ±95% confidence intervals.

RNA-Seq. A549^{cHSF1} cells were seeded at 7.5 x 10^4 cells/well in a 12-well plate in DMEM media. Cells were then treated with either 0.01 % DMSO or 1 μg/mL dox for 24 h. Cellular RNA was harvested using the RNeasy Plus Mini Kit with QIAshredder homogenization columns (Qiagen). RNA samples were quantified using an Advanced Analytical Fragment Analyzer. The initial steps were performed on a Tecan EVO150.10 ng of total RNA was used for library preparation. 3'DGE-custom primers 3V6NEXT-bmc#1-24 were added to a final concentration of 1 μM. (5'-/5Biosg/ACACTCTTTCCCTACACGACGCTCTTCCGATCT [BC6]N10T30VN-3' where 5Biosg = 5' biotin, [BC6] = 6bp barcode specific to each sample/well, N10 = Unique Molecular Identifiers, Integrated DNA technologies) were used to generate two subpools of 24 samples each[111, 112]. After addition of the oligonucleotides, Maxima H Minus RT was added per the manufacturer's recommendations with the template-switching oligo 5V6NEXT (10 μM,

[5V6NEXT : 5'-iCiGiCACACTCTTTCCCTACACGACGCrGrGrG-3' where iC: iso-dC, iG: iso-dG, rG: RNA G]), followed by incubation at 42 °C for 90 min and inactivation at 80 °C for 10 min. Following the template switching reaction, cDNA from 24 wells containing unique well identifiers were pooled together and cleaned using RNA Ampure beads at 1.0×. cDNA was eluted with 17 µL of water followed by digestion with Exonuclease I at 37 °C for 30 min, and inactivation at 80 °C for 20 min. Second strand synthesis and PCR amplification was done by adding the Advantage 2 Polymerase Mix (Clontech) and the SINGV6 primer (10 pM, Integrated DNA Technologies 5'-/5Biosg/ACACTCTTTCCCTACACGACGC-3') directly to half of the exonuclease reaction volume. Eight cycles of PCR were performed, followed by clean-up using regular SPRI beads at 0.6×, and elution with 20 µL of Resuspension Buffer (Illumina). Successful amplification of cDNA was confirmed using the Fragment Analyzer. Illumina libraries were then produced using Nextera FLEX tagmentation substituting P5NEXTPT5-bmc primer (25 µM, Integrated DNA Technologies, (5'-AATGATACGGCGACCACCGAGATCTACACTCTTTCCCTACACGACGCTCTTCCG*A*T*C*T*-3' where * = phosphorothioate bonds) in place of the normal N500 primer. Final libraries were cleaned using SPRI beads at 0.7× and quantified using the Fragment Analyzer and qPCR before being loaded for paired-end sequencing using the Illumina NextSeq500 in paired-end mode (26/50 nt reads).

Analyses were performed using previously described tools and methods[113]. Reads were aligned against hg19 (Feb., 2009) using bwa mem v. 0.7.12-r1039 [RRID:SCR_010910] with flags –t 16 –f, and mapping rates, fraction of multiply-mapping reads, number of unique 20-mers at the 5´ end of the reads, insert size distributions, and fraction of ribosomal RNAs were calculated using bedtools v. 2.25.0 [RRID:SCR_006646][114]. In addition, each resulting bam file was randomly down-sampled to a million reads, which were aligned against hg19, and read density across genomic features were estimated for RNA-Seq-specific quality control metrics. For mapping and quantitation, reads were scored against GRCh38/ENSEMBL 101 annotation using Salmon v.1.3 with flags quant -p 8 -l ISR –validateMappings[115]. The resulting quant.sf files were imported into the R statistical environment using the tximport library (tximport function, option "salmon"), and gene-level counts and transcript per-milllion (TPM) estimates were calculated for protein-coding genes. Samples were clustered based on genes with average log2 TPM >0.1 across all samples (n=6320 genes) based on complete linkage clustering of the Cosine correlation among samples. Samples with similarity score <0.94, which were clear outliers from the rest, were excluded from further analysis (n=5).

Differential expression was also analyzed in the R statistical environment (R v.3.5.1) using Bioconductor's DESeq2 package on the protein-coding genes only [RRID:SCR_000154][116]. Dataset parameters were estimated using the estimateSizeFactors(), and estimateDispersions() functions; read

counts across conditions were modeled based on a negative binomial distribution, and a Wald test was used to test for differential expression (nbinomWaldtest(), all packaged into the DESeq() function), using the treatment type as a contrast. Shrunken $\log_2$ fold-changes were calculated using the lfcShrink function, based on a normal shrinkage estimator[116]. Fold-changes and *p*-values were reported for each protein-coding gene. Upregulation was defined as a change in expression level >1.5-fold relative to the basal environment with a non-adjusted *p*-value < 10^{-5}. Gene ontology analyses were performed using the online DAVID server, according to tools and methods presented by Huang and co-workers[113].

Gene set enrichment analysis (GSEA). Differential expression results from DESeq2 were retrieved, and the "stat" column was used to pre-rank genes for GSEA analysis. These "stat" values reflect the Wald's test performed on read counts as modeled by DESeq2 using the negative binomial distribution. Genes that were not expressed were excluded from the analysis. GSEA (linux desktop version, v4.1)[117, 118] was run in the pre-ranked mode against MSigDB 7.4 C5 (Gene Ontology) set, and ENSEMBL IDs were collapsed to gene symbols using the Human_ENSEMBL_Gene_ID_MSigDB.v7.4.chip (resulting in 12706 unique genes for par and 12141 for sg4, respectively). In addition, a weighted scoring scheme, meandiv normalization, and cutoffs on MSigDB signatures sizes (between 5 and 2000 genes, resulting in 8496 gene sets retained) were applied and 5000 permutations were run for *p*-value estimation.

Generating A549^{cHSF1}(p53-Lib) cells. A549^{cHSF1} cells were infected with titered p53 library lentivirus at a multiplicity of infection of 0.25 (4×10^7 cells mixed with 1×10^7 lentiviral particles) in the presence of 8 µg/mL polybrene. Following transduction, cells were selected with 2 µg/mL puromycin (Gibco).

Deep mutational scanning. A549^{cHSF1}(p53-Lib) cells were seeded in 15 cm tissue culture plates at a density of 3×10^6 cells/plate. In order to maintain library diversity throughout selection, three plates were used per treatment for a total of 9×10^6 cells. Cells were treated with 0.01% DMSO, 1 µg/mL dox, 0.01% DMSO and 2.5 µM nutlin-3, or 1 µg/mL dox and 2.5 µM nutlin-3. Cells were trypsinized, counted, and re-seeded in three plates each at 3×10^6 cells/plate every 3 d. Following 12 d of treatment, cell pellets were harvested by centrifugation at 1,000 rpm for 5 min. Aliquots of 9×10^6 cells were snap-frozen in liquid N_2(g) in Eppendorf tubes and stored at –80 °C for subsequent DNA extraction. The deep mutational scanning experiment was repeated independently for a total of three biological replicates from the same p53-Lib cell line.

To prepare samples for Illumina sequencing, genomic DNA was purified from aliquots of frozen cells using the QIAamp Blood Midi Kit (Qiagen) and final DNA concentration was determined using a Qubit (Fischer). PCR amplicons of p53 were prepared using 2.0 µg of genomic DNA over 25 cycles and

with Herculase II as the DNA polymerase (Agilent). The primers used were 5' ATTCTCCTTGGAATTT-GCCCTT 3' and 5' CATAGCGTAAAAGGAGCAACA 3'. Twelve PCR reactions were performed per sample, and the reactions were pooled and cleaned up using a PCR clean-up kit (Omega). The p53 amplicons were further gel-purified using a Pippin prep system (Sage Science) prior to library preparation via Nextera Flex. The resulting libraries were quantified using the Fragment Analyzer before they were pooled and sequenced on an Illumina NovaSeq with 2 × 150 bp paired-end reads.

Deep mutational scanning data analysis. The software ORFCall v1.0 [https://github.com/broadinstitute/ORFCall/releases/tag/v1.0] was used with flags -p -Q 30 to align the deep-sequencing reads against the *TP53* wild-type sequence and count the number of times each codon mutation was observed in each selection condition. The mutational fold-change for each variant was calculated by normalizing raw read counts to the total read count at each position. Mutational fitness in each condition was determined by averaging the $\log_2$ fold-change in selection versus mock conditions from three biological replicates. RSA was calculated using the software DSSP on chain A of the p53 DNA-binding domain crystal structure (PDBID 2OCJ)[119, 120]. DSSP calculates the solvent-accessible surface area of the monomer (ASA) and the RSA is calculated by dividing the ASA by the total theoretical solvent accessibility area[121]. Sites were classified as buried if the RSA was <0.2 and exposed if the RSA was >0.2.

Rosetta analysis. The calculations for $\Delta\Delta G$ of protein stability upon substitution were performed using the cartesian_ddg application in Rosetta version 3.13[91]. The crystal structure of the DNA-binding domain of p53 (PDB ID: 2OCJ, chain A) was used as the initial structure for the $\Delta\Delta G$ calculations[120]. The initial p53 structure was relaxed using the Rosetta FastRelax application to generate a total of 20 relaxed decoys. The Rosetta FastRelax application performed five cycles of side-chain repacking and energy minimization with the Rosetta energy function ref2015_cart[91, 122-124]. The lowest energy structure of the 20 decoys was used as the wild-type structure for the cartesian_ddg calculation. In the cartesian_ddg calculation, the target residue was substituted with each of the 20 natural amino acids, and any neighboring residues within a 9-Å radius were repacked and energy-minimized using the ref2015_cart energy function. This calculation process was performed five times to generate five energy scores for the mutant and for the wild-type. The average wild-type scores were subtracted from the average mutant scores to calculate the $\Delta\Delta G$ values. The $\Delta\Delta G$ values were then scaled by a factor of 0.34; this scale factor was previously calculated by fitting Rosetta-predicted $\Delta\Delta G$ values to experimental $\Delta\Delta G$ values in units of kcal/mol, and is used here to better relate predicted $\Delta\Delta G$ values to experimental values[91].

Statistical analyses. All experiments were performed in biological triplicate. All statistical analyses calculations were done in Jupyter Notebook. Site and mutational $\log_2$ fold-change (**Figure 2**) were calculated using a Wilcoxon signed-rank test. Statistical significance in mutational $\log_2$ fold-change in missense mutations and buried versus exposed sites (**Figures S2C**, **S2D**, **S6B**, **S6D**, and **4B**) were calculated using a Welch's *t*-test for independent samples with Bonferroni correction, and significance from null was determined using a Wilcoxon signed-rank test. All correlations were determined by calculating Pearson correlation coefficients using a two-tailed test. The statistical significance between solvent RSA classes or mutation types within a solvent accessibility class (**Figures 4C** and **4D**) was evaluated using ANOVA, while comparisons between select conditions were calculated using Welch's *t*-test for independent samples with Bonferroni correction. Statistical significance between stabilizing and destabilizing mutations based on experimental measurements (**Figure 5A**) as well as for significance between buried and exposed regions (**Figure 5B**) was calculated using a Welch's *t*-test for independent variables. ANOVA was also used to calculate statistical significance between RSA class and amino acid changes and $\Delta\Delta G$ (**Figures 5E** and **5F**).

References

1. Ostroverkhova, D., Przytycka, T.M. & Panchenko, A.R. Cancer driver mutations: Predictions and reality. *Trends Mol Med.* **29**, 554-566 (2023).
2. Hanahan, D. & Weinberg, R.A. The hallmarks of cancer. *Cell* **100**, 57-70 (2000).
3. Hanahan, D. & Weinberg, R.A. Hallmarks of cancer: The next generation. *Cell* **144**, 646-674 (2011).
4. Nagel, R., Semenova, E.A. & Berns, A. Drugging the addict: Non-oncogene addiction as a target for cancer therapy. *Embo Rep* **17**, 1516-1531 (2016).
5. Luo, J., Solimini, N.L. & Elledge, S.J. Principles of cancer therapy: Oncogene and non-oncogene addiction. *Cell* **136**, 823-837 (2009).
6. Whitesell, L. & Lindquist, S.L. HSP90 and the chaperoning of cancer. *Nat Rev Cancer* **5**, 761-772 (2005).
7. Dufey, E., Urra, H. & Hetz, C. ER proteostasis addiction in cancer biology: Novel concepts. *Semin Cancer Biol* **33**, 40-47 (2015).
8. Dai, C.K., Dai, S.Y. & Cao, J.Y. Proteotoxic stress of cancer: Implication of the heat-shock response in oncogenesis. *J Cell Physiol* **227**, 2982-2987 (2012).
9. Guang, M.H.Z. et al. Targeting proteotoxic stress in cancer: A review of the role that protein quality control pathways play in oncogenesis. *Cancers* **11** (2019).
10. Mayer, M.P. et al. Stress biology: Complexity and multifariousness in health and disease. *Cell Stress Chaperones* **29**, 143-157 (2024).
11. Bagratuni, T. et al. XBP1s levels are implicated in the biology and outcome of myeloma mediating different clinical outcomes to thalidomide-based treatments. *Blood* **116**, 250-253 (2010).
12. Chen, X. et al. XBP1 promotes triple-negative breast cancer by controlling the HIF1alpha pathway. *Nature* **508**, 103-107 (2014).
13. Akerfelt, M., Morimoto, R.I. & Sistonen, L. Heat shock factors: Integrators of cell stress, development and lifespan. *Nat Rev Mol Cell Biol.* **11**, 545-555 (2010).
14. Alasady, M.J. & Mendillo, M.L. The multifaceted role of HSF1 in tumorigenesis. *Adv Exp Med Biol.* **1243**, 69-85 (2020).
15. Mendillo, M.L. et al. HSF1 drives a transcriptional program distinct from heat shock to support highly malignant human cancers. *Cell* **150**, 549-562 (2012).
16. Scherz-Shouval, R. et al. The reprogramming of tumor stroma by HSF1 is a potent enabler of malignancy. *Cell* **158**, 564-578 (2014).
17. Santagata, S. et al. Tight coordination of protein translation and HSF1 activation supports the anabolic malignant state. *Science* **341**, 1238303 (2013).
18. Cyran, A.M. & Zhitkovich, A. Heat shock proteins and HSF1 in cancer. *Front Oncol.* **12**, 860320 (2022).
19. Dai, C., Whitesell, L., Rogers, A.B. & Lindquist, S. Heat shock factor 1 is a powerful multifaceted modifier of carcinogenesis. *Cell* **130**, 1005-1018 (2007).
20. Smith, R.S. et al. HSF2 cooperates with HSF1 to drive a transcriptional program critical for the malignant state. *Sci Adv.* **8** (2022).
21. Min, J.N., Huang, L., Zimonjic, D.B., Moskophidis, D. & Mivechi, N.F. Selective suppression of lymphomas by functional loss of HSF1 in a p53-deficient mouse model for spontaneous tumors. *Oncogene* **26**, 5086-5097 (2007).
22. Santagata, S. et al. High levels of nuclear heat-shock factor 1 (HSF1) are associated with poor prognosis in breast cancer. *PNAS* **108**, 18378-18383 (2011).
23. Whitesell, L. et al. HSP90 empowers evolution of resistance to hormonal therapy in human breast cancer models. *PNAS* **111**, 18297-18302 (2014).

24. Desai, S. et al. Heat shock factor 1 (HSF1) controls chemoresistance and autophagy through transcriptional regulation of autophagy-related protein 7 (ATG7). *J Biol Chem.* **288**, 9165-9176 (2013).
25. Nikolaou, M., Pavlopoulou, A., Georgakilas, A.G. & Kyrodimos, E. The challenge of drug resistance in cancer treatment: A current overview. *Clin Exp Metastasis* **35**, 309-318 (2018).
26. Birbo, B., Madu, E.E., Madu, C.O., Jain, A. & Lu, Y. Role of HSP90 in cancer. *Int J Mol Sci.* **22** (2021).
27. Li, Z.N. & Luo, Y. HSP90 inhibitors and cancer: Prospects for use in targeted therapies (Review). *Oncol Rep.* **49** (2023).
28. Lang, J.E. et al. Safety and efficacy of HSP90 inhibitor ganetespib for neoadjuvant treatment of stage II/III breast cancer. *NPJ Breast Cancer* **8**, 128 (2022).
29. Rodina, A. et al. The epichaperome is an integrated chaperome network that facilitates tumour survival. *Nature* **538**, 397-401 (2016).
30. Dong, B. et al. Targeting therapy-resistant prostate cancer via a direct inhibitor of the human heat shock transcription factor 1. *Sci Transl Med.* **12** (2020).
31. Salamanca, H.H., Antonyak, M.A., Cerione, R.A., Shi, H. & Lis, J.T. Inhibiting heat shock factor 1 in human cancer cells with a potent RNA aptamer. *PLoS One* **9**, e96330 (2014).
32. Vilaboa, N. et al. New inhibitor targeting human transcription factor HSF1: Effects on the heat shock response and tumor cell survival. *Nucleic Acids Res.* **45**, 5797-5817 (2017).
33. Pasqua, A.E. et al. HSF1 pathway inhibitor clinical candidate (CCT361814/NXP800) developed from a phenotypic screen as a potential treatment for refractory ovarian cancer and other malignancies. *J Med Chem.* **66**, 5907-5936 (2023).
34. Yoon, J., Patrick, J.E., Ogbunugafor, C.B. & Shoulders, M.D. Viral evolution shaped by host proteostasis networks. *Annu Rev Virol.* **10**, 77-98 (2023).
35. DePristo, M.A., Weinreich, D.M. & Hartl, D.L. Missense meanderings in sequence space: A biophysical view of protein evolution. *Nat Rev Genet.* **6**, 678-687 (2005).
36. Tokuriki, N. & Tawfik, D.S. Chaperonin overexpression promotes genetic variation and enzyme evolution. *Nature* **459**, 668-673 (2009).
37. Rutherford, S.L. & Lindquist, S. Hsp90 as a capacitor for morphological evolution. *Nature* **396**, 336-342 (1998).
38. Geller, R., Pechmann, S., Acevedo, A., Andino, R. & Frydman, J. Hsp90 shapes protein and RNA evolution to balance trade-offs between protein stability and aggregation. *Nat Commun.* **9**, 1781 (2018).
39. Karras, G.I. et al. HSP90 shapes the consequences of human genetic variation. *Cell* **168**, 856-866 e812 (2017).
40. Phillips, A.M. et al. Host proteostasis modulates influenza evolution. *eLife* **6** (2017).
41. Phillips, A.M. et al. Enhanced ER proteostasis and temperature differentially impact the mutational tolerance of influenza hemagglutinin. *eLife* **7** (2018).
42. Phillips, A.M. et al. Destabilized adaptive influenza variants critical for innate immune system escape are potentiated by host chaperones. *PLoS Biol.* **16**, e3000008 (2018).
43. Yoon, J. et al. The endoplasmic reticulum proteostasis network profoundly shapes the protein sequence space accessible to HIV envelope. *PLoS Biol.* **20**, e3001569 (2022).
44. Nekongo, E.E. et al. HSF1 activation can restrict HIV replication. *ACS Infect Dis.* **6**, 1659-1666 (2020).
45. Yoon, J. et al. The immune-evasive proline-283 substitution in influenza nucleoprotein increases aggregation propensity without altering the native structure. *Sci Adv.* **10**, eadl6144 (2024).
46. Mantovani, F., Collavin, L. & Del Sal, G. Mutant p53 as a guardian of the cancer cell. *Cell Death Differ.* **26**, 199-212 (2019).
47. Mendiratta, G. et al. Cancer gene mutation frequencies for the U.S. population. *Nat Commun.* **12**, 5961 (2021).

48. Baugh, E.H., Ke, H., Levine, A.J., Bonneau, R.A. & Chan, C.S. Why are there hotspot mutations in the TP53 gene in human cancers? *Cell Death Differ.* **25**, 154-160 (2018).
49. Zhang, C. et al. Gain-of-function mutant p53 in cancer progression and therapy. *J Mol Cell Biol.* **12**, 674-687 (2020).
50. Boettcher, S. et al. A dominant-negative effect drives selection of TP53 missense mutations in myeloid malignancies. *Science* **365**, 599-604 (2019).
51. Gencel-Augusto, J. & Lozano, G. p53 tetramerization: At the center of the dominant-negative effect of mutant p53. *Genes Dev.* **34**, 1128-1146 (2020).
52. De Vries, A. et al. Targeted point mutations of p53 lead to dominant-negative inhibition of wild-type p53 function. *PNAS* **99**, 2948-2953 (2002).
53. Bullock, A.N., Henckel, J. & Fersht, A.R. Quantitative analysis of residual folding and DNA binding in mutant p53 core domain: Definition of mutant states for rescue in cancer therapy. *Oncogene* **19**, 1245-1256 (2000).
54. Bullock, A.N. et al. Thermodynamic stability of wild-type and mutant p53 core domain. *PNAS* **94**, 14338-14342 (1997).
55. Ang, H.C., Joerger, A.C., Mayer, S. & Fersht, A.R. Effects of common cancer mutations on stability and DNA binding of full-length p53 compared with isolated core domains. *J Biol Chem.* **281**, 21934-21941 (2006).
56. Cho, Y., Gorina, S., Jeffrey, P.D. & Pavletich, N.P. Crystal structure of a p53 tumor suppressor-DNA complex: Understanding tumorigenic mutations. *Science* **265**, 346-355 (1994).
57. Whitesell, L., Sutphin, P.D., Pulcini, E.J., Martinez, J.D. & Cook, P.H. The physical association of multiple molecular chaperone proteins with mutant p53 is altered by geldanamycin, an HSP90-binding agent. *Mol Cell Biol.* **18**, 1517-1524 (1998).
58. Dahiya, V. et al. Coordinated conformational processing of the tumor suppressor protein p53 by the HSP70 and HSP90 chaperone machineries. *Mol Cell* **74**, 816-830 e817 (2019).
59. Boysen, M., Kityk, R. & Mayer, M.P. HSP70- and HSP90-mediated regulation of the conformation of p53 DNA binding domain and p53 cancer variants. *Mol Cell* **74**, 831-843 e834 (2019).
60. Muller, L., Schaupp, A., Walerych, D., Wegele, H. & Buchner, J. Hsp90 regulates the activity of wild type p53 under physiological and elevated temperatures. *J Biol Chem.* **279**, 48846-48854 (2004).
61. Muller, P., Hrstka, R., Coomber, D., Lane, D.P. & Vojtesek, B. Chaperone-dependent stabilization and degradation of p53 mutants. *Oncogene* **27**, 3371-3383 (2008).
62. Wiech, M. et al. Molecular mechanism of mutant p53 stabilization: The role of HSP70 and MDM2. *PLoS One* **7**, e51426 (2012).
63. Peng, Y., Chen, L., Li, C., Lu, W. & Chen, J. Inhibition of MDM2 by Hsp90 contributes to mutant p53 stabilization. *J Biol Chem.* **276**, 40583-40590 (2001).
64. Blagosklonny, M.V., Toretsky, J., Bohen, S. & Neckers, L. Mutant conformation of p53 translated in vitro or in vivo requires functional HSP90. *PNAS* **93**, 8379-8383 (1996).
65. Li, D. et al. Functional inactivation of endogenous MDM2 and CHIP by HSP90 causes aberrant stabilization of mutant p53 in human cancer cells. *Mol Cancer Res.* **9**, 577-588 (2011).
66. Giard, D.J. et al. In vitro cultivation of human tumors: establishment of cell lines derived from a series of solid tumors. *J Natl Cancer Inst.* **51**, 1417-1423 (1973).
67. Lehman, T.A. et al. p53 mutations, ras mutations, and p53-heat shock 70 protein complexes in human lung carcinoma cell lines. *Cancer Res.* **51**, 4090-4096 (1991).
68. Sebastian, R.M. & Shoulders, M.D. Chemical Biology Framework to Illuminate Proteostasis. *Annu Rev Biochem.* **89**, 529-555 (2020).
69. Voellmy, R. Dominant-positive and dominant-negative heat shock factors. *Methods* **35**, 199-207 (2005).
70. Moore, C.L. et al. Transportable, chemical genetic methodology for the small molecule-mediated inhibition of Heat Shock Factor 1. *ACS Chem Biol.* **11**, 200-210 (2016).

71. Ryno, L.M. et al. Characterizing the altered cellular proteome induced by the stress-independent activation of heat shock factor 1. *ACS Chem Biol.* **9**, 1273-1283 (2014).
72. Liebelt, F. et al. SUMOylation and the HSF1-Regulated Chaperone Network Converge to Promote Proteostasis in Response to Heat Shock. *Cell Rep.* **26**, 236-249 e234 (2019).
73. Kovacs, D. et al. HSF1Base: A comprehensive database of HSF1 (heat shock factor 1) target genes. *Int J Mol Sci.* **20** (2019).
74. Ying, W. et al. Ganetespib, a unique triazolone-containing Hsp90 inhibitor, exhibits potent antitumor activity and a superior safety profile for cancer therapy. *Mol Cancer Ther.* **11**, 475-484 (2012).
75. Riss, T.L. et al. in Assay Guidance Manual (Bethesda (MD); 2004).
76. Giacomelli, A.O. et al. Mutational processes shape the landscape of TP53 mutations in human cancer. *Nat Genet.* **50**, 1381-1387 (2018).
77. Shen, H. & Maki, C.G. Pharmacologic activation of p53 by small-molecule MDM2 antagonists. *Curr Pharm Des.* **17**, 560-568 (2011).
78. Bouaoun, L. et al. TP53 variations in human cancers: New lessons from the IARC TP53 database and genomics data. *Hum Mutat.* **37**, 865-876 (2016).
79. Doud, M.B. & Bloom, J.D. Accurate measurement of the effects of all amino-acid mutations on influenza hemagglutinin. *Viruses* **8** (2016).
80. Haddox, H.K., Dingens, A.S. & Bloom, J.D. Experimental estimation of the effects of all amino-acid mutations to HIV's envelope protein on viral replication in cell culture. *PLoS Pathog.* **12**, e1006114 (2016).
81. Lee, J.M. et al. Deep mutational scanning of hemagglutinin helps predict evolutionary fates of human H3N2 influenza variants. *PNAS* **115**, E8276-E8285 (2018).
82. Joerger, A.C. & Fersht, A.R. Structural biology of the tumor suppressor p53. *Annu Rev Biochem.* **77**, 557-582 (2008).
83. Butler, J.S. & Loh, S.N. Structure, function, and aggregation of the zinc-free form of the p53 DNA binding domain. *Biochemistry* **42**, 2396-2403 (2003).
84. Blanden, A.R. et al. Zinc shapes the folding landscape of p53 and establishes a pathway for reactivating structurally diverse cancer mutants. *eLife* **9** (2020).
85. Pradhan, M.R. et al. Simulations of mutant p53 DNA binding domains reveal a novel druggable pocket. *Nucleic Acids Res.* **47**, 1637-1652 (2019).
86. Natan, E. et al. Interaction of the p53 DNA-binding domain with its N-terminal extension modulates the stability of the p53 tetramer. *J Mol Biol.* **409**, 358-368 (2011).
87. Soragni, A. et al. A Designed Inhibitor of p53 Aggregation Rescues p53 Tumor Suppression in Ovarian Carcinomas. *Cancer Cell* **29**, 90-103 (2016).
88. Joerger, A.C., Ang, H.C., Veprintsev, D.B., Blair, C.M. & Fersht, A.R. Structures of p53 cancer mutants and mechanism of rescue by second-site suppressor mutations. *J Biol Chem.* **280**, 16030-16037 (2005).
89. Nikolova, P.V., Henckel, J., Lane, D.P. & Fersht, A.R. Semirational design of active tumor suppressor p53 DNA binding domain with enhanced stability. *PNAS* **95**, 14675-14680 (1998).
90. Nikolova, P.V., Wong, K.B., DeDecker, B., Henckel, J. & Fersht, A.R. Mechanism of rescue of common p53 cancer mutations by second-site suppressor mutations. *EMBO J.* **19**, 370-378 (2000).
91. Park, H. et al. Simultaneous optimization of biomolecular energy functions on features from small molecules and macromolecules. *J Chem Theory Comput.* **12**, 6201-6212 (2016).
92. Liberzon, A. et al. The Molecular Signatures Database (MSigDB) hallmark gene set collection. *Cell Syst.* **1**, 417-425 (2015).
93. Prieto, C. & De Las Rivas, J. APID: Agile Protein Interaction DataAnalyzer. *Nucleic Acids Res.* **34**, W298-302 (2006).

94. Willis, A., Jung, E.J., Wakefield, T. & Chen, X. Mutant p53 exerts a dominant negative effect by preventing wild-type p53 from binding to the promoter of its target genes. *Oncogene* **23**, 2330-2338 (2004).
95. Milner, J. & Medcalf, E.A. Cotranslation of activated mutant p53 with wild type drives the wild-type p53 protein into the mutant conformation. *Cell* **65**, 765-774 (1991).
96. Kennedy, M.C. & Lowe, S.W. Mutant p53: It's not all one and the same. *Cell Death Differ.* **29**, 983-987 (2022).
97. Pfister, N.T. & Prives, C. Transcriptional regulation by wild-type and cancer-related mutant forms of p53. *Cold Spring Harb Perspect Med.* **7** (2017).
98. Kaida, A. & Iwakuma, T. Regulation of p53 and cancer signaling by heat shock protein 40/J-domain protein family members. *Int J Mol Sci.* **22** (2021).
99. Finlay, C.A. et al. Activating mutations for transformation by P53 produce a gene-product that forms an Hsc70-P53 complex with an altered half-life. *Mol Cell Biol.* **8**, 531-539 (1988).
100. Li, J. et al. Amyloid aggregates induced by the p53-R280T mutation lead to loss of p53 function in nasopharyngeal carcinoma. *Cell Death Dis.* **15**, 35 (2024).
101. Isermann, T. et al. Suppression of HSF1 activity by wildtype p53 creates a driving force for p53 loss-of-heterozygosity. *Nat Commun.* **12**, 4019 (2021).
102. Li, D., Yallowitz, A., Ozog, L. & Marchenko, N. A gain-of-function mutant p53-HSF1 feed forward circuit governs adaptation of cancer cells to proteotoxic stress. *Cell Death Dis.* **5**, e1194 (2014).
103. Gould, S.I. et al. High-throughput evaluation of genetic variants with prime editing sensor libraries. *Nat Biotechnol.* (2024).
104. Dai, C. & Sampson, S.B. HSF1: Guardian of proteostasis in cancer. *Trends Cell Biol.* **26**, 17-28 (2016).
105. Solimini, N.L., Luo, J. & Elledge, S.J. Non-oncogene addiction and the stress phenotype of cancer cells. *Cell* **130**, 986-988 (2007).
106. Kim, S.H. et al. Suppression of multidrug resistance via inhibition of heat shock factor by quercetin in MDR cells. *Exp Mol Med.* **30**, 87-92 (1998).
107. Tchenio, T., Havard, M., Martinez, L.A. & Dautry, F. Heat shock-independent induction of multidrug resistance by heat shock factor 1. *Mol Cell Biol.* **26**, 580-591 (2006).
108. Vilaboa, N.E., Galan, A., Troyano, A., de Blas, E. & Aller, P. Regulation of multidrug resistance 1 (MDR1)/P-glycoprotein gene expression and activity by heat-shock transcription factor 1 (HSF1). *J Biol Chem.* **275**, 24970-24976 (2000).
109. Vydra, N., Toma, A., Glowala-Kosinska, M., Gogler-Piglowska, A. & Widlak, W. Overexpression of Heat Shock Transcription Factor 1 enhances the resistance of melanoma cells to doxorubicin and paclitaxel. *BMC Cancer* **13**, 504 (2013).
110. Jaeger, A.M. et al. Rebalancing Protein Homeostasis Enhances Tumor Antigen Presentation. *Clin Cancer Res* **25**, 6392-6405 (2019).
111. Soumillon, M., Cacchiarelli, D., Semrau, S., van Oudenaarden, A. & Mikkelsen, T.S. Characterization of directed differentiation by high-throughput single-cell RNA-Seq *bioRxiv* (2014).
112. Struntz, N.B. et al. Stabilization of the max homodimer with a small molecule attenuates myc-driven transcription. *Cell Chem Biol.* **26**, 711-723 e714 (2019).
113. Huang, D.W., Sherman, B.T. & Lempicki, R.A. Bioinformatics enrichment tools: Paths toward the comprehensive functional analysis of large gene lists. *Nucleic Acids Res.* **37**, 1-13 (2009).
114. Quinlan, A.R. & Hall, I.M. BEDTools: A flexible suite of utilities for comparing genomic features. *Bioinformatics* **26**, 841-842 (2010).
115. Patro, R., Duggal, G., Love, M.I., Irizarry, R.A. & Kingsford, C. Salmon provides fast and bias-aware quantification of transcript expression. *Nat Methods* **14**, 417-419 (2017).
116. Love, M.I., Huber, W. & Anders, S. Moderated estimation of fold change and dispersion for RNA-seq data with DESeq2. *Genome Biol.* **15**, 550 (2014).

117. Subramanian, A. et al. Gene set enrichment analysis: A knowledge-based approach for interpreting genome-wide expression profiles. *PNAS* **102**, 15545-15550 (2005).
118. Mootha, V.K. et al. PGC-1alpha-responsive genes involved in oxidative phosphorylation are coordinately downregulated in human diabetes. *Nat Genet.* **34**, 267-273 (2003).
119. Kabsch, W. & Sander, C. Dictionary of protein secondary structure: Pattern recognition of hydrogen-bonded and geometrical features. *Biopolymers* **22**, 2577-2637 (1983).
120. Wang, Y., Rosengarth, A. & Luecke, H. Structure of the human p53 core domain in the absence of DNA. *Acta Crystallogr D Biol Crystallogr.* **63**, 276-281 (2007).
121. Tien, M.Z., Meyer, A.G., Sydykova, D.K., Spielman, S.J. & Wilke, C.O. Maximum allowed solvent accessibilites of residues in proteins. *PLoS One* **8**, e80635 (2013).
122. Maguire, J.B. et al. Perturbing the energy landscape for improved packing during computational protein design. *Proteins* **89**, 436-449 (2021).
123. Alford, R.F. et al. The Rosetta all-atom energy function for macromolecular modeling and design. *J Chem Theory Comput.* **13**, 3031-3048 (2017).
124. Khatib, F. et al. Algorithm discovery by protein folding game players. *PNAS* **108**, 18949-18953 (2011).

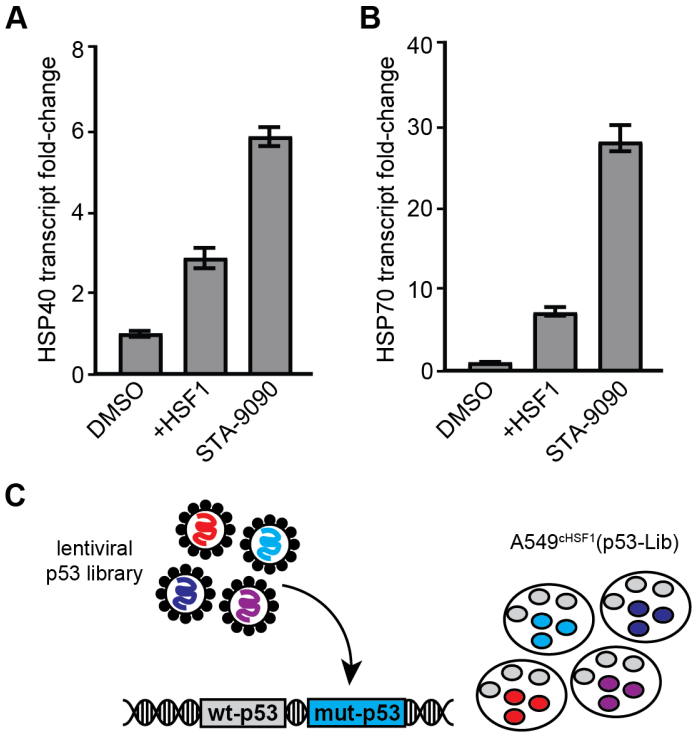

Figure 1: Validation of dox-mediated HSF1 regulation and construction of the A549^{cHSF1}(p53-Lib) cell line.

qPCR results showing transcript-level consequences of dox-mediated HSF1 activation for the HSF1 target genes (**A**) HSP40 and (**B**) HSP70 in A549^{cHSF1} cells. Treatment with the HSP90 inhibitor STA-9090 was used as a positive control for HSR activation, and to ensure pathways were activated within the regime accessible to endogenous HSF1 transcriptional activity. (**C**) Creation of A549^{cHSF1}(p53-Lib) cells: A549 cells expressing endogenous wild-type p53 were transduced at a low multiplicity of infection with a lentiviral population encoding all possible single amino acid substitutions within *TP53.*

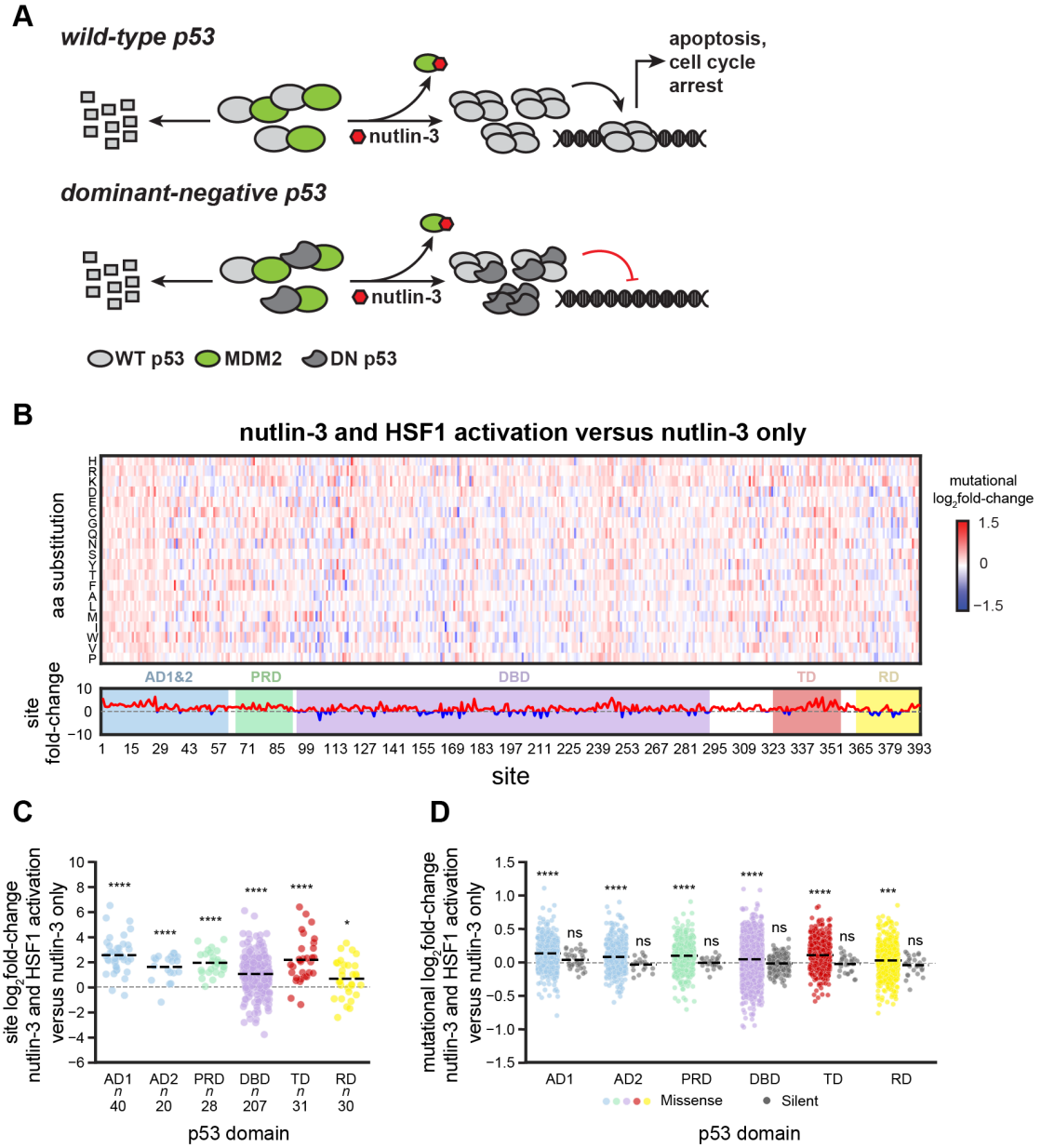

Figure 2: HSF1 activation enhances mutational fitness of dominant-negative p53 variants. (**A**) Selection of dominant-negative variants using nutlin-3. Treatment with nutlin-3 prevents MDM2-mediated degradation of both wild-type and mutant p53. Co-expression of dominant-negative p53 variants prevents induction of cell cycle arrest by endogenous wild-type p53, thereby allowing cell proliferation. (**B**) Heat map of the p53 mutational frequency $\log_2$ fold-change averaged over three biological replicates for each amino acid substitution for nutlin-3-mediated dominant-negative p53 selection in an HSF1-activated environment as compared to nutlin-3-mediated dominant-negative p53 selection in a basal proteostasis environment. The sum of the mutational $\log_2$ fold-change at each site is shown below. (**C**) Total site $\log_2$ fold-change for amino acid substitutions in the selection conditions in (**B**) subdivided across each p53 domain. (**D**) Log_2 fold-change for each individual DNA-level mutation in the *TP53* gene subdivided for each domain, presented here for the selection conditions in (**B**) and separating missense (*red*) from synonymous mutations (*grey*). Significance was calculated using a Wilcoxon signed-rank test, with *, ***, and **** representing adjusted two-tailed *p*-values of <0.05, <0.001, and <0.0001, respectively, and ns

indicating non-significant. AD1, activation domain 1; AD2, activation domain 2; PRD, proline-rich domain; DBD, DNA-binding domain; TD, tetramerization domain; RD, regulatory domain.

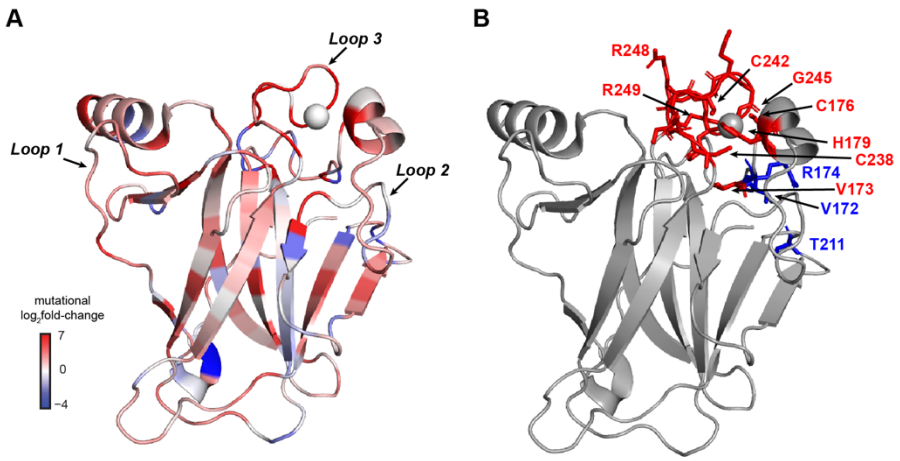

Figure 3: HSF1 activation in the context of nutlin-3-mediated selection alters mutational fitness within the p53 DNA-binding domain.
(**A**) Structure of the p53 DNA-binding domain (PDB 2OCJ). Residues are colored according to the net site $\log_2$ fold-change. (**B**) Consequences of HSF1 activation at selected, individually labeled hotspot sites associated with cancer. Color indicates net positive (*red*) or negative (*blue*) site $\log_2$ fold-change.

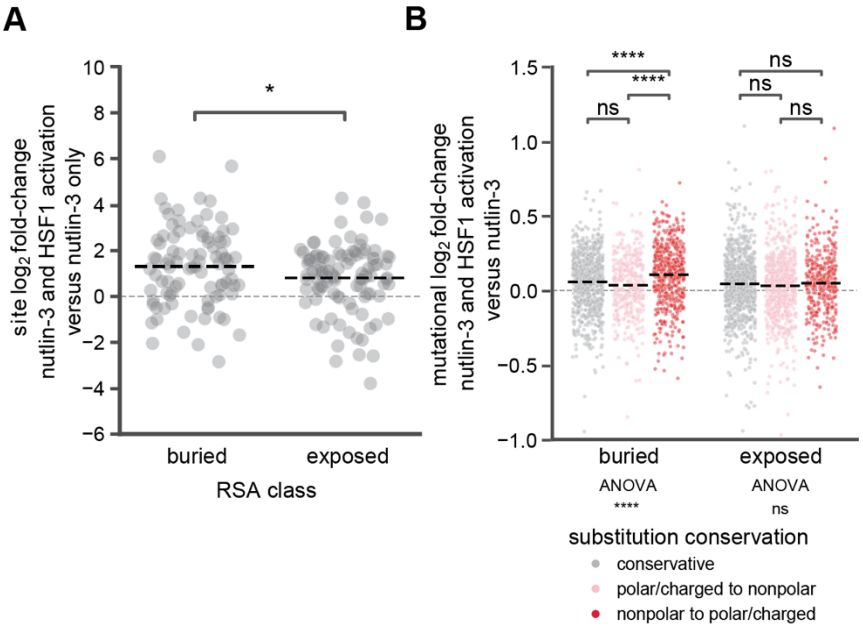

Figure 4: HSF1 activation specifically increases tolerance for charged mutations in buried regions of p53.

(**A**) Average net site $\log_2$ fold-change across the p53 DNA-binding domain for sites classified as buried (relative solvent accessibility or RSA < 0.2) versus exposed (RSA > 0.2). (**B**) Mutational $\log_2$ fold-change in variant fitness for conservative amino acid substitutions, non-conservative non-polar to polar substitutions, and non-conservative polar to non-polar substitutions at buried versus accessible sites in p53. Statistical significance between solvent accessibility classes or mutation types within a solvent accessibility class was evaluated using ANOVA, while comparisons between select conditions were calculated using Welch's *t*-test for independent samples with Bonferroni correction. *, ***, and **** represent adjusted two-tailed *p*-values of <0.05, <0.001, and <0.0001, respectively.

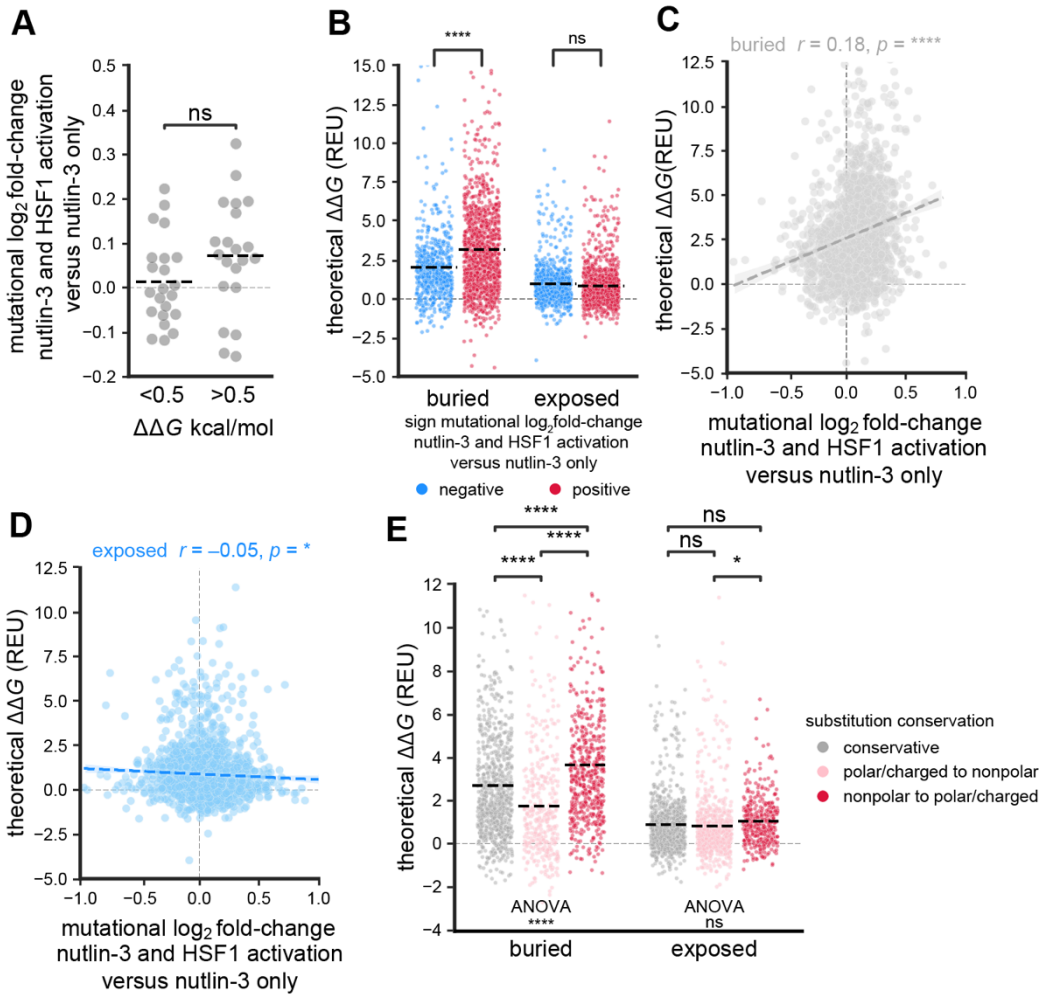

Figure 5: HSF1 activation most strongly enhances the fitness of destabilizing p53 amino acid substitutions within the DNA-binding domain.
(**A**) Average mutational $\log_2$ fold-change for nutlin-3 selection in HSF1-activated versus basal proteostasis environments for variants classified as stabilizing or wild-type-like ($\Delta\Delta G$ < 0.5 kcal/mol) versus destabilizing ($\Delta\Delta G$ > 0.5 kcal/mol), based on experimental thermodynamic stability measurements. (**B**) Theoretical $\Delta\Delta G$ calculated using Rosetta analysis (REU = Rosetta energy units) for p53 DNA-binding domain substitutions in buried, partially exposed or exposed sites. Variants are binned into those that displayed either a positive or a negative average $\log_2$ fold-change in HSF1-activated versus basal proteostasis environments during nutlin-3 selection. Correlation plots comparing average mutational $\log_2$ fold-change for nutlin-3 selection in HSF1-activated versus basal proteostasis environments for buried (**C**) and exposed (**D**) sites as compared to Rosetta $\Delta\Delta G$ calculated values. Pearson correlation coefficients r as well as the corresponding p-values are included. (**E**) $\Delta\Delta G$ calculations suggest that amino acids in buried regions are less tolerant to non-conservative (nonpolar to polar/charged) substitutions than sites in exposed regions. These are the same types of substitutions whose fitness was most substantially enhanced by HSF1 activation (**Figure 4B**). Statistical significance was evaluated using Welch's t-test for independent samples with Bonferroni correction, with *, **, ***, and **** representing adjusted two-tailed p-values of <0.05 and <0.0001, respectively.

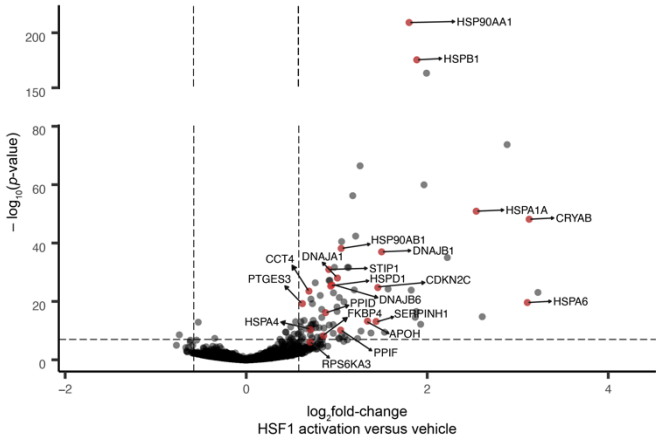

Figure 6: HSF1-activated genes and known p53-interacting proteins overlap.
Volcano plot for RNA-Seq analysis of changes in gene transcription following HSF1 activation in A549^{cHSF1} cells as compared to vehicle treatment. Proteins within the Agile Protein Interaction DataAnalyzer (APID) that have been identified as interactors with p53 are labeled and shown in red.